Original Article

JCBFM

Journal of Cerebral Blood Flow & Metabolism
0(00) 1–10

DOI: 10.1177/0271678X17732275
journals.sagepub.com/home/jcbfm
SAGE

Higher prevalence of spontaneous cerebral vasculopathy and cerebral infarcts in a mouse model of sickle cell disease

Hyacinth I Hyacinth[1,*], Courtney L Sugihara[2], Thomas L Spencer[3], David R Archer[1] and Andy Y Shih[4,5,*]

Abstract

Stroke is a dramatic complication of sickle cell disease (SCD), which is associated with cerebral vasculopathies including moya moya, intravascular thrombi, cerebral hyperemia, and increased vessel tortuosity. The spontaneous occurrence of these pathologies in the sickle cell mouse model has not been described. Here, we studied Townes humanized sickle cell and age-matched control mice that were 13 months old. We used in vivo two-photon microscopy to assess blood flow dynamics, vascular topology, and evidence of cerebral vasculopathy. Results showed that compared to controls, sickle cell mice had significantly higher red blood cell (RBC) velocity (0.73 mm/s vs. 0.55 mm/s, $p = 0.013$), capillary vessel diameter (4.84 μM vs. 4.50 μM, $p = 0.014$), and RBC volume flux (0.015 nL/s vs. 0.010 nL/s, $p = 0.021$). Also, sickle cell mice had significantly more tortuous capillary vessels ($p < 0.0001$) and significantly shorter capillary vessel branches ($p = 0.0065$) compared to controls. Sickle cell mice also had significantly higher number of capillary occlusive events (3.4% vs. 1.9%, $p < 0.0001$) and RBC stalls (3.8% vs. 2.1%, $p < 0.0001$) in the cerebral capillary bed. In post-mortem immunohistochemical analyses, sickle cell mice had a 2.5-fold higher frequency of cortical microinfarcts compared to control mice. Our results suggest that aged Townes sickle cell mice spontaneously develop SCD-associated cerebral vasculopathy.

Keywords

Sickle cell disease, stroke, cerebral vasculopathy, cerebral blood flow, hematology

Received 30 January 2017; Revised 24 August 2017; Accepted 25 August 2017

Introduction

In homozygous sickle cell disease (SCD), the substitution of valine for glutamic acid in the beta chain of the globin portion of the hemoglobin molecule forms sickle hemoglobin.[1] Sickle hemoglobin polymerizes during conditions of hypoxemia, leadizng to defective erythrocytes that are fragile and easily lysed.[2] The resulting chronic hemolysis and anemia are accompanied not only by exuberant erythropoiesis with increased catabolism and protein synthesis in the individual,[3] but also by chronic inflammation secondary to ongoing vascular endothelial injury and recurrent vaso-occlusive events.[4,5]

Animal models of SCD offer valuable opportunities to test therapeutic interventions and to understand the biological basis for the complications of SCD, with each model possessing its own strengths and

[1]Department of Pediatrics, Aflac Cancer and Blood Disorder Center of Children's Healthcare of Atlanta and Emory University, Atlanta, GA, USA
[2]Neuroscience and Behavioral Biology Program, Emory University, Atlanta, GA, USA
[3]Department of Mechanical Engineering, Georgia Technical Institute, Atlanta, GA, USA
[4]Department of Neurosciences, Medical University of South Carolina, Charleston, SC, USA
[5]Center for Biomedical Imaging, Medical University of South Carolina, Charleston, SC, USA
*These authors contributed equally to this work.

Corresponding author:
Hyacinth I Hyacinth, Department of Pediatrics, Aflac Cancer and Blood Disorder Center of Children's Healthcare of Atlanta and Emory University, 2015 Uppergate Dr., Atlanta, GA 30045, USA.
Email: hhyacinth@emory.edu

weaknesses.[6] Since its introduction, the Berkeley transgenic sickle cell mouse model has served well for the study of some features of human SCD, especially chronic erythrocyte sickling, tissue hypoxia, hemolytic anemia, and extramedullary hematopoiesis.[7] In addition, it has also been very useful for studying SCD complications such as sickle cell chronic lung disease, bone marrow infarction or embolization, retinopathy, renal papillary necrosis or splenic atrophy.[8] A limitation of this model is the lack of a humanized (mouse model which expresses exclusively human α-, β-, and/or γ-globins) control. The observed histopathological changes of chronic tissue hypoxia and hemolytic anemia in the Berkeley model include infarcts and siderosis in the spleen, kidneys, and liver;[9] as well as, splenomegaly secondary[8] to exuberant extramedullary hematopoiesis. Manci et al.[8] previously stated that while the Berkeley transgenic sickle cell mice modeled very closely many aspects of human SCD, they failed to show spontaneous cerebrovascular pathology such as cerebral vasculopathy or infarcts, which has been well documented as a complication of SCD in humans. In a recent review, Hillery and Panepinto[10] reported that SCD is associated with microvascular cerebral vasculopathy, which might require time to develop in the SCD mouse model, possibly because of the inherent anatomical difference between the cerebral vascular bed in humans and mice.

Here, we used in vivo two-photon laser-scanning microscopy[11] to study and describe spontaneous cerebral microvascular changes in humanized Townes sickle cell and control mice that were 13 months old at the time of experimentation.[11] Previous reports that sickle cell mice lacked spontaneous cerebrovascular changes were from studies in mice with an age range of between one and six months.[8] We hypothesized that with age, Townes sickle cell mice will spontaneously develop cerebral vasculopathy which will be more severe compared to controls. We showed that aged (13 months old) Townes mice do indeed develop cerebral vasculopathy and as such might be a useful model for in vivo studies of spontaneous cerebral vasculopathy and cerebrovascular disease in SCD. In addition, this model system is a potentially useful platform for development and testing of drugs for the prevention SCD-associated cerebrovascular disease.

Methods

Animal preparation

The Institution Animal Care and Use Committees (IACUC) of Emory University and the Medical University of South Carolina, approved this study. All research was conducted in accordance with the National Research Council and National Institutes of Health *Guide for the Care and Use of Laboratory Animals 8th Edition*.[12] Reporting of methods, results and all aspects of this paper are in accordance with appropriate reporting standard (ARRIVE). Reporting of methods was based on the recommendations from the *Quality of methods reporting in animal models of colitits*.[13]

This is a cross-sectional study utilizing the Townes mouse model, a humanized sickle cell (with HbSS) and corresponding control (with HbAA) mouse model. A total of 10, 13 months old, male mice, 5 each of HbAA and HbSS were transferred from Emory University's Pediatrics animal facility to the Medical University of South Carolina, where all imaging studies were conducted. The mice were allowed to acclimatize for one week before surgery and imaging. After acclimatization, the mice were transferred to the laboratory in pairs for surgery. At both Institution's animal facilities, mice were housed with a 12-h light/dark cycle; water and feed were provided ad libitum. Each transgenic SCD mouse was processed and imaged alongside an age-matched HbAA mouse. We have previously described the methods for preparing and imaging the cerebral vasculature of mice using in vivo two-photon laser scanning microscopy.[14,15] Random group assignment of the mice was not necessary because grouping was based on the genotype of the mouse, i.e. sickle cell or "wild-type"/control mouse, respectively. But to control for potential differences between imaging sessions, we randomly decided whether a sickle cell mouse or control will be experimented (surgery and imaging) on in the morning and which will be experimented on in the afternoon.

The mice were anesthetized using 2% isoflurane (Patterson Veterinary) in pure oxygen in an induction chamber. They were then transferred to the operating stage where isoflurane was delivered through a nose cone and an adequate depth of anesthesia was maintained via titration based on the response of the mouse to a slight paw pinch. The skin was cleaned with betadine and then the cranial bone exposed. The periosteum was gently removed using fine dissecting tools under a dissecting microscope and then dental cement was used to affix a custom-made metal flange for head stabilization during imaging, and to form a head cap to protect the cut skin. A heating pad set at 37°C was used to maintain constant body temperature based on bio-feedback from an attached thermal probe.

Using a fine drill (Osada, Los Angeles, CA) and 0.5 mm drill burr (Fine Science Tools, Foster City, CA), a craniotomy was gently made by removing an approximately 3 mm × 3 mm piece of skull bone overlying the sensory cortex. The skull bone and subsequently the pial surface were constantly moistened with

artificial cerebrospinal fluid to avoid desiccation. Agarose gel was placed around the cranial window and a no. 0 glass coverslip laid over the window to overlap slightly the edge of the window. The glass slide was secured with dental cement before imaging was started.

In vivo imaging procedure

Two-photon imaging was performed with a Sutter Moveable Objective Microscope (MOM) and a Coherent Ultra II Ti:Sapphire laser source. Mice were maintained under an appropriate level of isoflurane (0.5–1.0%) supplied in air (20–22% oxygen and 78% nitrogen, moisturized by bubbling through water) over the duration of imaging. Further, mice were given an intraperitoneal injection of 500 μL of saline before commencing imaging in order to reduce the risk of dehydration during imaging. The plasma was labeled by an intravenous injection of 0.03 mL of 2 MDa fluorescein-dextran (FD2000S; Sigma-Aldrich) prepared at a concentration of 5% (w/v) in sterile saline.[14,15] Procedures for blood flow imaging and analysis have been described previously.[15] Wide-field images were collected using a 4×, 0.13 NA objective lens (Olympus UPLFLN 4×) to generate vascular maps of the entire window for navigational purposes. High-resolution imaging of microvessels was performed by using a 20×, 1.0 NA objective lens (Olympus XLUMPLFLN 20×W). High-resolution image stacks of the vasculature were collected across a 326 by 326 μm field and up to a depth of 400–500 μm from the pial surface. Lateral sampling was 0.3 to 0.6 μm per pixel and axial sampling was at 1 μm steps between frames.

All measurements of cerebral vasodynamic and microvascular parameters were obtained using in vivo two-photon blood flow imaging, with methods that were previously described.[15,16]

Immunohistochemistry

At the conclusion of two-photon imaging, animals were allowed to fully recover from anesthesia, and then given Hypoxyprobe intravenously (see below). They were then sacrificed 1 h later. Animals were perfuse fixed with 4% (w/v) paraformaldehyde in PBS. Brain were extracted and post-fixed overnight at 4°C. In each mouse, the entire brain was sectioned because the infarcts were spontaneous and we did not know a priori, the location of infarcts. Brain sections were collected at a thickness of 50 μm and stored in PBS with 0.2% sodium azide. Anti-NeuN primary antibody from guinea pig host (ABN90; Millipore, Billerica, MA) was diluted in buffer consisting of 10% (v/v) goat serum (Vector Labs), 2% (v/v) Triton X-100 and 0.2% (w/v) sodium azide. Free-floating sections were then incubated overnight under slow nutation at room temperature. The following day, sections were washed in 50 mL of PBS for 30 min on an orbital shaker, incubated with an anti-mouse Alexa 594 secondary antibody for 2 ho, washed again in PBS, mounted, and dried on slides for 30 min. All slides were then sealed with Fluoromount-G (Southern Biotechnology Associates Inc.) and a No. 1 glass coverslip (Corning). Staining for other targets such as CD31 (550274 BD Biosciences) for the endothelium used a similar protocol as above. For pimonidazole hydrochloride (HP3-100 Kit, Hypoxyprobe™; Hypoxyprobe.com) immunostaining of hypoxic tissue,[17] pimonidazole was injected via the retro-orbital route 1 h prior to sacrifice at a concentration of 60 mg/kg dissolved in saline and given at a volume of 100 μL per mouse. The bound hypoxyprobe adduct is detected using a rabbit anti-hypoxyprobe antibody. Finally, cell nuclei were labeled by adding Hoescht 33342 (Sigma-Aldrich) at a ratio of 1:100 in secondary antibody solution, 10–30 min prior to washing. Quantification of frequency of microinfarcts was done in 20 similarly located but non-consecutive 50 μM brain sections obtained from a region between 3.08 mm anterior and 1.94 mm posterior to the bregma. Sections were labeled with a combination of anti-mouse NeuN, Hypoxyprobe, and FITC or anti-mouse NeuN, anti-mouse CD31, and FITC. We defined a microinfarct as one that was $\geq$50 μM in diameter. Because we did not observe any of the classical symptoms of stroke (such hemiparesis) in our mice, we did not define any of the cerebral infarcts as a stroke irrespective of the size. The definition of microinfarct was also based on our prior findings from occlusion of a single penetrating arteriole.[18]

Microvessel analysis

Vessel masking. Image volumes (161 × 161 × 100 μm), collected with two-photon microscopy, were processed into binary masks using ImageJ software.[19,20] Separate masks were created for skeletonization and vessel volume analysis, respectively. Processing of images occurred in the following order for each analysis:

Vascular volume mask. (1) Image converted to 8-bit. (2) 3D smoothing of the 8-bit image utilizing a Gaussian filter with sigma set to 1.0. (3) Thresholding of image to include all pixels between the intensity values of 15 to 355. (4) Creation of a binary mask based on the thresholded image. (5) 3D erosion algorithm with an isovalue of 155, applied three times to more accurately reflect the space occupied by the intraluminal dye. Using custom MATLAB software, the volume occupied by voxels with a value of 1 was divided by the volume of

all voxels examined, i.e. 0 and 1. The calculated value may under-estimate the total intravascular volume since blood cells are not labeled by the FITC-dextran dye.

Microvessel skeletonization. (1) Image converted to 8-bit. (2) 3D smoothing of the image utilizing a Gaussian filter with sigma set to 1.0. (3) Thresholding of image to include all pixels of between the intensity values of 15 to 355. (4) Creation of binary mask based on the thresholded image. (5) A $5 \times 5 \times 5\,\mu m$, 3D median filter was applied to the binary mask to eliminate noise. (6) 3D skeletonization algorithm was run on the filtered binary mask. "Skeletonize (3D)" (http://fiji.sc/Skeletonize3D) and "Analyze Skeleton" (http://fiji.sc/AnalyzeSkeleton) plugins for Fiji software were used for these procedures. (7) Vessel segments with branch lengths of less than $5\,\mu m$, the average diameter of a capillary, were removed to eliminate branches fabricated by the skeletonization algorithm when vessels of larger diameter, i.e. $>10\,\mu m$, were present in the image stack. (8) Using custom MATLAB and BoneJ plugins, the microvascular branch volume, length, and Euclidean distance between the tips of branch points were determined.

Quantification of vasodynamic and intravascular cellular parameters. User defined line scans,[16] videos, and Z-stacks obtained from each mouse from each genotype group were analyzed, using custom MATLAB codes and Fiji/Image J software. Z-stacks were analyzed for: (1) the proportion of capillary vessels with intravascular occlusive events (defined a priori as an unlabeled intravascular object that is 10× or more the diameter of an red blood cell (RBC) which is $\sim 7.5\,\mu m$ (Supplemental Figure 1(a)), (2) the proportion of capillary vessels with blood flow stalls, defined as a total cessation of blood flow on z-stacks or videos and (3) the number of RBCs arrested, defined as an RBC that is stationary for 1 or more second, expressed per unit time and unit length of capillary vessel segment (Supplemental Figure 1(b)). Further, line scans were analyzed to quantify RBC velocity using custom MATLAB codes.[21] Capillary diameter was manually measured using ImageJ software. RBC flux was calculated using the formula[17]

$$F = \left({}^{1}/_{8}\right)\pi \times v \times d^{2}$$

where F is the RBC volume flux (cortical blood flow) through a vessel segment in nL/s, v is the velocity of RBC and d is the diameter of the vessel. Although a technical limitation of the above formula is that it assumes laminar flow which is not the case in capillaries which have "single file flow," but nevertheless allows an estimation of the impact of lumen diameter changes co-occurring with RBC velocity change. Euclidean distance, a measure of vessel tortuosity and the average microvascular branch length were obtained from the analysis of skeletonized 3D image reconstruction of the z-stacks.

Image processing, statistical considerations, and data analysis. Image processing, analysis and scaling, and video processing were done using the combination of Adobe CS6 (Adobe Systems Co., San Jose, CA), Fiji/Image J,[20] and Microsoft Movie Maker (Microsoft® Corp. Redmond, WA). All image processing and analysis were performed in a blinded fashion by a coauthor (CLS) who was not aware of the genotype or group assignment of the mice at the time.

Data analysis for comparison between sickle cell and control mice was done using the GraphPad Prism software (GraphPad Software Inc., La Jolla, CA). Data were checked for normality using the Shapiro–Wilk test and then the Mann–Whitney U-test was used for comparison between sickle cell and control mice because of the heteroscedasticity in our data based on Levene's F-test for equality of variance. Since this was an exploratory study, we did not formally perform an a priori sample size calculation. Our study sample size was chosen as five mice per genotype group based on our prior experiments and publications using this mouse model.[22–24] We had noted from prior experiments that a minimum of four mice in each genotype group was needed to show a statistically significant difference in end organ damage score between sickle cell mice and controls. Quantitative results are presented using bar dot plots, comparing sickle to control mice and with a p-value of <0.05 considered statistically significant. Qualitative data are presented as representative videos or an array of histochemical images.

Results

Cerebrovascular morphology and cerebral vasodynamics in sickle cell compared to control mice

All animals included in the study were analyzed for the results presented below. We used 13 months old male Townes sickle cell and control mice in this study. Analysis of cerebral vasodynamic measurements revealed that sickle cell mice had significantly higher capillary RBC velocity (0.73 mm/s vs. 0.55 mm/s, $p = 0.013$) compared to controls (Figure 1(a)). In addition, sickle cell mice also had significantly larger capillary vessel diameter ($4.84\,\mu M$ vs. $4.50\,\mu M$, $p = 0.014$) compared to controls (Figure 1(b)). Since RBC volume flux is a function of vessel diameter and

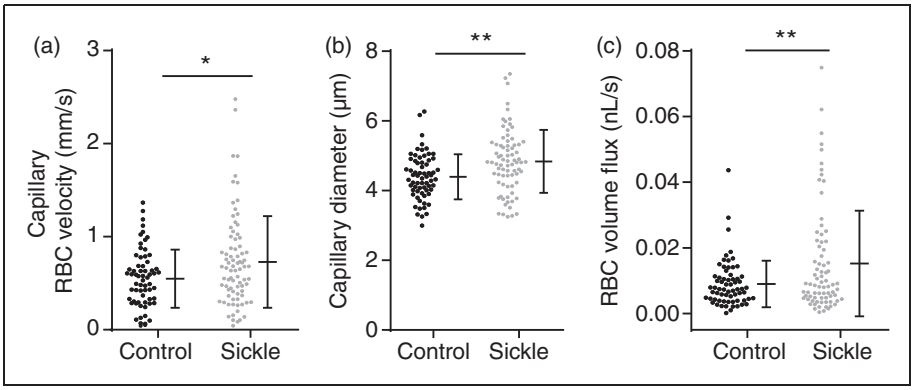

Figure 1. Altered capillary vasodynamics in the sickle cell compared to control mice. Red blood cell velocity (a), mean capillary diameter (b), and red blood cell flux (c) were significantly higher among sickle cell mice compared with controls ($p = 0.013$, 0.014, 0.021 for RBC velocity, capillary diameter, and flux, respectively; Mann–Whitney U-test). Error bars represent mean ± SD, $1-\beta = 0.92$ in (a), 0.95 in (b), and 0.99 in (c).

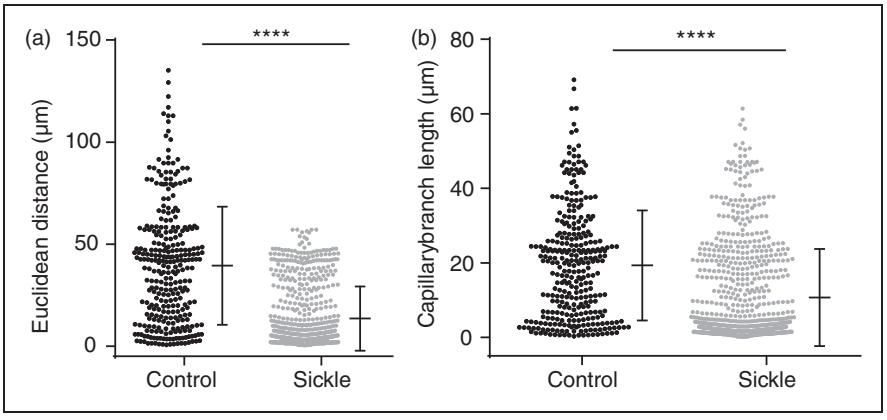

Figure 2. Abnormal capillary topology in the sickle cell compared to control mice. (a) The Euclidean between branch points, an indication of the degree of vessel tortuosity, was significantly shorter in sickle cell mice ($p < 0.0001$, Mann–Whitney test). (b) Sickle cell mice also have significantly shorter capillary branch length compared to controls ($p = 0.0065$, Mann–Whitney U-test). Error bars represent mean ± SD, $1 - \beta = 0.99$ in (a) and 0.99 in (b).

RBC velocity, sickle cell mice had significantly higher RBC volume flux (0.015 nL/s vs. 0.010 nL/s, $p = 0.021$) compared to controls (Figure 1(c)).

Sickle cell mice also had gross evidence of altered cerebrovascular topology (Supplemental Video 2(a) to (d)). Specifically, we determined the Euclidean distance of capillary branch-points, i.e. the 3D distance between two branch-point vertices, which has been shown to indicate the level of tortuosity of a vessel.[25,26] The average Euclidean distance was significantly shorter in sickle cell mice (13.5 μm vs. 39.5 μm, $p < 0.0001$) compared to controls (Figure 2(a)), indicating that the sickle cell mice had significantly more tortuous capillary network. Consistent with this, the average capillary length was also significantly shorter in sickle cell (10.6 μm vs. 19.3 μm, $p = 0.0065$) compared to control mice (Figure 2(b)).

Sickle cell mice have significantly more spontaneous intravascular pathologies

Using images from line scans and 3D image stacks, an assessor (C.L.S) who was blinded to the genotype of the mice counted the number of vessels with occlusive events (clots or adherent cells that were ≥10× the size of an RBC; Supplemental Video 3(a) for control mouse and, Supplemental Video 3(b) for sickle cell mouse) or RBC stalls (capillary segments with stationary RBCs). These measurements were then expressed as a percentage of the total number of vessels examined (Figure 3). Sickle cell mice had a significantly higher percentage of cerebral vessels with occlusive events (3.4% vs. 1.9%, $p < 0.0001$) per image field compared to controls (Figure 3(a)). Similarly, sickle cell mice had significantly higher percentage of vessels with RBC flow

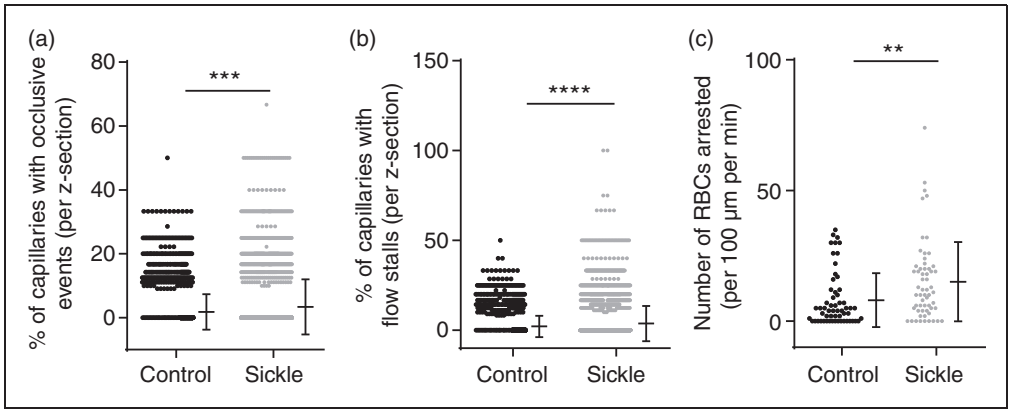

Figure 3. Higher prevalence and severity of evidence of cerebral vasculopathy in the sickle cell mice compared to controls. (a) Higher number of occlusive events ($p < 0.001$) (b) blood flow stalls ($p < 0.0001$) and (c) arrested RBCs ($p = 0.036$) were observed in sickle cell, compared to control mice. Comparison done using Mann–Whitney U-test and error bars represent mean ± SD, $1-\beta = 0.99$ in (a), 0.99 in (b), and 0.95 in (c). Note that in Figure 3(a), 2940 out of 3296 and 3298 out of 3900 data points for controls and sickle mice respectively have a value of zero percent. And in Figure 3(b), 2872 out of 3300 and 3287 out of 3900 data points also have a value of zero percent.

stalls (3.8% vs. 2.1%, $p < 0.0001$) compared to controls (Figure 3(b)). Consistent with the higher incidence of flow stalls in sickle cell mice, there was a significantly greater number of arrested RBCs (20.8 vs. 13.6, $p = 0.036$) per 100 µm of vessel length per minute, among sickle cell mice compared to controls (Figure 3(c)). An arrested RBC was defined as one that remained motionless for 1 s or longer.

Significantly higher prevalence of spontaneous cortical microinfarcts in sickle cell mice

After completion of two-photon imaging, mice were injected intravenously with Hypoxyprobe, a marker that binds tissues with less than 10 mmHg pO_2 content, providing an immunohistochemical target for identifying hypoxic brain regions. Brains were then extracted, sectioned, and immunolabeled for Hypoxyprobe, along with markers of neuronal viability, NeuN, and endothelial cells, CD31. The occurrence of cortical microinfarcts was a prominent feature in the brains of sickle cell mice (Figure 4). Microinfarcts manifested as localized regions devoid of NeuN immunoreactivity, indicating loss of neuronal viability (Figure 4(a) and (d); left panels). They closely resembled the column-like shape of microinfarcts induced by direct occlusion of cortical penetrating arterioles or venules in the mouse brain.[27] We also observed microinfarcts in aged controls, although they were smaller in area and significantly less frequent compared to sickle cell mice (Figure 4). Furthermore, supportive of the idea that spontaneous microinfarcts arise from the blockage of cortical penetrating vessels, we observed changes consistent with a tissue response to ischemia. This included: (i) local extravasation of the intravenous fluorescent dye, FITC-dextran, confirming blood–brain barrier leakage (Figure 4(a), (b), and (e); right panels), (ii) increased binding of Hypoxyprobe in the microinfarct core (Figure 4(c) and (d); right panels), and (iii) local degeneration of the vascular endothelium (Figure 4(e); left panel). We assessed the frequency of microinfarcts (≥50 µM in diameter) in each group by examining all brain sections from sickle cell (N = 5) and control (N = 5) mice, encompassing ~20 sections per mouse spanning the entire cerebrum. This revealed an average of 2.5-fold higher frequency of microinfarcts in the brain of sickle cell mice compared to that of controls. Similarly, as shown in Figure 4(g), the average area of cortical infarcts was significantly larger in sickle cell ($0.05 \pm 0.05\,mm^2$) compared to control ($0.009 \pm 0.01\,mm^2$) mice ($p = 0.0021$).

Discussion

In this study, we showed that aged Townes sickle cell mice spontaneously develop cerebrovascular pathologies that are akin to those seen in human SCD. The observance of cerebral vasculopathy in children with SCD prompted prior efforts to study the cerebral vasculature of sickle cell mice that were six months old or younger.[8] However, cerebrovascular disease in general, is an age-related phenomenon, and thus the goal of this study was to examine cerebrovascular function and pathology in an aged sickle cell mouse model and to compare it with matched controls.

We observed a significantly higher capillary RBC velocity in sickle cell mice compared to controls, which recapitulates what had been demonstrated in

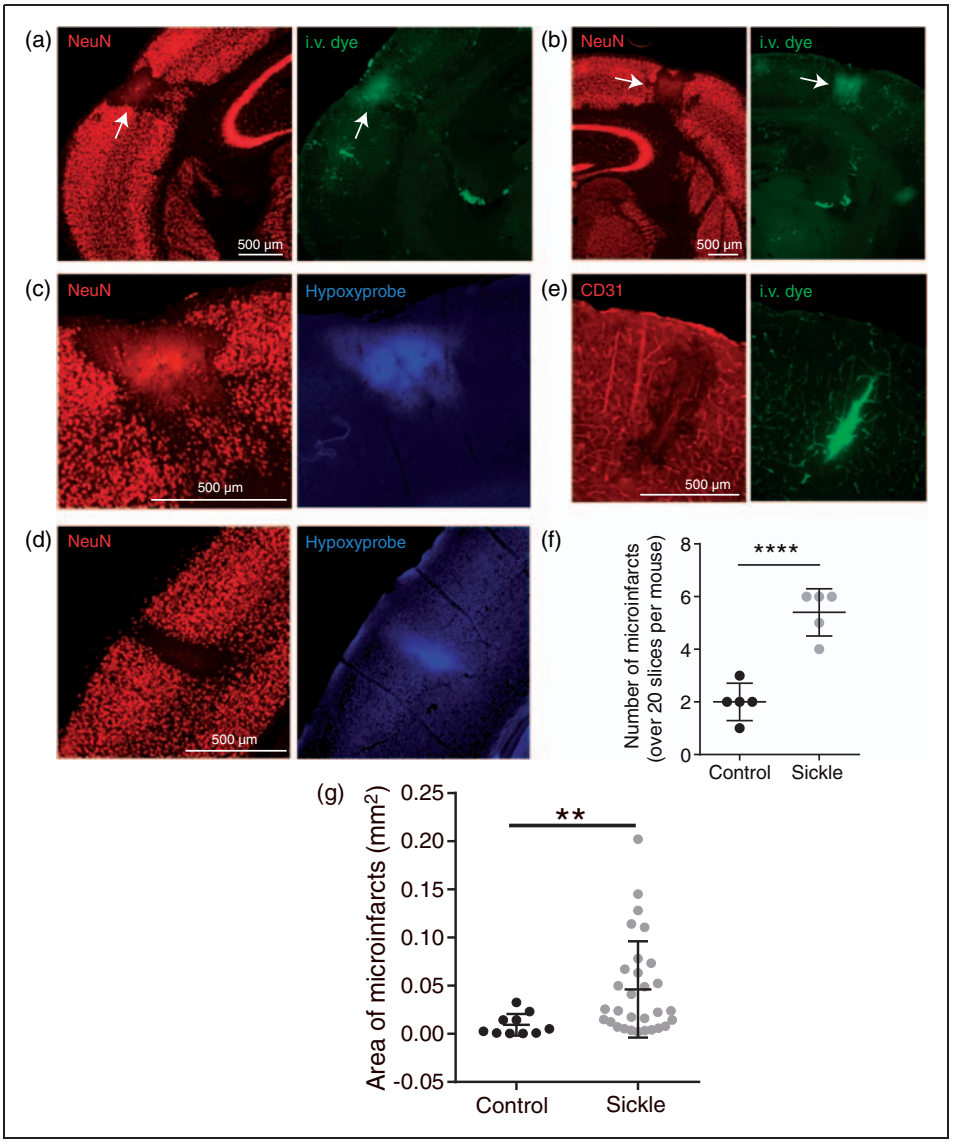

Figure 4. Higher frequency of spontaneous cerebral microinfarcts in the sickle cell compared to control mice. Representative images of cortical microinfarcts in sickle cell (a, b and c) and control (d) mice. Regions devoid of NeuN staining, a marker of neuronal viability, mark the boundaries of the microinfarcts. Extravasation of the intravenous dye, FITC-dextran, in and around the microinfarct core is consistent with blood–brain barrier disruption. (c, d) Hypoxyprobe labeling marks regions of tissue hypoxia. (e) CD31 staining for endothelial cells, showing endothelial damage in the microinfarct core where there was also leakage of FITC. (f) Sickle cell mice had a 2.5-fold higher frequency of microinfarcts compared to control mice ($p < 0.0001$). (g) Finally, sickle cell mice had significantly larger average area of infarct compared to controls ($p = 0.0021$). Comparison between groups was performed using Mann–Whitney U-test and error bars represent mean ± SD, $1-\beta = 0.99$ in (f) and 0.94 in (g).

children and adults with SCD.[28,29] This increase in RBC velocity is thought to reflect increased compensatory cardiac output. However, we also observed a slight dilation of brain capillaries in sickle cell mice, which would reduce blood flow resistance and also increase velocity. A high RBC velocity is associated with shortened RBC transit time, which could negatively impact oxygen extraction, with significant neurological consequences as seen in SCD.[28,30–32] In addition, we noted that sickle cell mice have greater vascular tortuosity and significantly shortened vessel branches. These structural changes may contribute to the greater number of RBC stalls we observed in the capillary beds of sickle cell mice. Our finding of shorter vessel branches supports earlier reported observations of ineffective collateral vessel formation, also known as moya moya.[33] Moya moya refers to short tufts of blood vessels that are ineffective in perfusing localized cerebral

tissue despite their increased number. They have been associated with a significantly increased risk for stroke among individuals with SCD.[34] Our study supports this finding in humans given that the sickle cell mice had both shortened and tortuous vessels as well as a higher frequency of cortical microinfarcts.

One key observation was that sickle cell mice had a 2.5-fold increased frequency of cerebral microinfarcts compared with controls. The exact relationship between this finding and above reported capillary level vascular topological and vasodynamic differences between sickle cell and control mice is still unknown and will be the subject of further studies in our laboratory. Overall, cerebral infarcts were cortical in location. Among the sickle cell mice, about two-thirds of microinfarcts were observed between the rostral and bregmatic region, with the rest observed after the bregma (Figure 4), while there was no observable pattern in the location of the infarcts among controls. Another important observation was the significantly higher prevalence of cerebral intravascular occlusive events in sickle cell compared to control mice. These cerebral vaso-occlusive events resemble the peripheral vaso-occlusive events that are the hallmark of SCD and could conceivably be partially responsible for the cortical microinfarcts. We also observed multiple ''thrombi'' circulating in the sickle cell mice in vivo but not in the control mice. The clinical significance of this finding is still unknown since a similar observation has not been reported in children or adults with SCD. But a recent study reports that individuals who were heterozygous for the sickle cell mutation (i.e. having sickle cell trait), have an increased risk for atrial fibrillation[35] and in the context of vascular cognitive impairment, atherosclerosis or atrial fibrillation can lead to the generation of microthrombi that circulate into the brain to occlude cerebral small vessels.[36,37] This is thought to be a source of microinfarcts in the aging brain, and may also play a role in development of microinfarcts in SCD. Since microinfarcts have recently been linked to an increased risk for dementia,[38] it is possible that the accumulation of these lesions may also contribute to cognitive decline in SCD.[39–41] A surprising finding was the observation of spontaneous cerebral infarcts among the control mice (Figure 4(d)). We reasoned that this might be a consequence of the age (13 months at time of experiment) of the control mice we used in this study. But, as earlier stated, the frequency of cortical microinfarcts was still significantly higher among sickle cell mice compared to age-matched controls. Finally, we noted that the average area of microinfarcts was significantly larger in sickle cell compared to control mice. We report this observation with the caution that we do not know the age of the infarcts in sickle cell or control mice, making a true comparison difficult. But given our knowledge of the pathobiology of SCD, and this mouse model, we do not expect the control mice to have microinfarcts at an earlier age compared to sickle cell mice. This is because if the infarcts occurred earlier in controls, they would have had more time to heal and involute, thus reducing their size. Our discussion on these microinfarcts is limited by the fact that we did not ascertain their origin. However, their remarkable resemblance to microinfarcts induced by the occlusion of single penetrating arterioles or perhaps venules by photothrombosis,[42] suggests that they may arise from the occlusion of penetrating arterioles or venules by one or more pathobiological processes in SCD. Further, the detection of local hypoxic tissue suggests that microinfarcts in sickle cell mice are likely a consequence of vascular occlusion. Future studies are needed to determine the role of vascular adhesion molecule and other mediators of macro and microvascular remodeling in the etiology of spontaneous cerebral microinfarcts in SCD.

A limitation of our study is the fact that it is a cross-sectional study and as such we are unable to make any solid claims of causality or mechanisms. But we did observe in our model, pathologies that have been reported to be associated with high incidence of stroke in humans with SCD. Further, we were not able to document clinical stroke symptoms in our model. A possible reason could be that a stroke severe enough to generate clinical symptoms would result in mortality due to dehydration (animal unable to drink) or aggression from cage mates. In addition, the size of the infarcts we documented on histology is too small to induce perceptible sensorimotor deficits. However, observing spontaneous microinfarcts is significant because of the well-established link between microinfarcts and cognitive function in humans with SCD. This later point is the subject of ongoing studies in our laboratory. These limitations do not diminish the significance of our findings, which show the presence of spontaneous cerebrovascular pathologies in an aged sickle cell mouse model, thus providing a tool for mechanistic and drug development studies.

In conclusion, we have shown the utility of a new approach to study the cerebrovascular consequences of SCD, using a combination of in vivo two-photon laser microscopy with post-mortem immunohistochemistry in an aged sickle cell mouse model. Using this approach, we have been able to measure abnormalities in microvascular blood flow and structure associated with SCD with high precision. This model system has potential for the longitudinal study of structural and molecular events involved in the evolution of SCD-associated cerebrovascular diseases and also for drug discovery.

Data and laboratory requests

Request for data used in manuscript can be made to our lab and we will oblige and share our raw data within the limits permissible that will not put us in a disadvantaged position as a laboratory. Mouse models are available from The Jackson Laboratories and we have provided within the manuscript, the sources of our reagents.

Funding

The author(s) disclosed receipt of the following financial support for the research, authorship, and/or publication of this article: This study was partially funded by grants to H. I. H from Emory University Pediatrics Pilot Grant (HeRO) and NIH/NHLBI (U01HL117721, R01HL138423). Also, grants to A.Y.S. from the NINDS (R21NS085402, R01NS097775), the Dana Foundation, a Charleston Conference on Alzheimer's Disease New Vision Award, South Carolina Clinical and Translational Institute (UL1TR000062), and an Institutional Development Award (IDeA) from the NIGMS under grant number P20GM12345.

Declaration of conflicting interests

The author(s) declared no potential conflicts of interest with respect to the research, authorship, and/or publication of this article.

Authors' contributions

HIH designed the experiment, HIH, CLS, TLS, DRA and AYS performed experiments and data analysis, HIH wrote the manuscript and CLS, TLS, DRA and AYS provided critical review. HIH and AYS performed final critical review. All authors endorsed the submission of this manuscript.

Supplementary material

Supplementary material for this paper can be found at the journal website: http://journals.sagepub.com/home/jcb

References

1. Pauling L and Itano HA. Sickle cell anemia a molecular disease. *Science* 1949; 110: 543–548.
2. Aster JC. Disease of organs systems: red blood cells and bleeding disorders – sickle cell disease. In: Vinay K, Fausto N and Abbas AK (eds) *Robins and cotran pathologic basis of disease*, 7 ed. Philadelphia: Elselvier Saunders, 2005, pp.628–632.
3. Hibbert JM, Creary MS, Gee BE, et al. Erythropoiesis and myocardial energy requirements contribute to the hypermetabolism of childhood sickle cell anemia. *J Pediat Gastroenterol Nutr* 2006; 43: 680–687.
4. Belcher JD, Bryant CJ, Nguyen J, et al. Transgenic sickle mice have vascular inflammation. *Blood* 2003; 101: 3953–3959.
5. Hibbert JM, Hsu LL, Bhathena SJ, et al. Proinflammatory cytokines and the hypermetabolism of children with sickle cell disease. *Exp Biol Med* 2005; 230: 68–74.
6. Fabry ME. Transgenic animal models of sickle cell disease. *Cell Mol Life Sci* 1993; 49: 28–36.
7. Pászty C, Brion CM, Manci E, et al. Transgenic knockout mice with exclusively human sickle hemoglobin and sickle cell disease. *Science* 1997; 278: 876–878.
8. Manci EA, Hillery CA, Bodian CA, et al. Pathology of Berkeley sickle cell mice: similarities and differences with human sickle cell disease. *Blood* 2006; 107: 1651–1658.
9. Manci EA, Hyacinth HI, Capers PL, et al. High protein diet attenuates histopathologic organ damage and vascular leakage in transgenic murine model of sickle cell anemia. *Exp Biol Med* 2014; 239: 966–974.
10. Hillery CA and Panepinto JA. Pathophysiology of stroke in sickle cell disease. *Microcirculation* 2004; 11: 195–208.
11. Tsai PS and Kleinfeld D. In vivo two-photon laser scanning microscopy with concurrent plasma-mediated ablation: principles and hardware realization. In: Frostig RD (ed.) *Methods for in vivo optical imaging*, 2 ed. Boca Raton, FL: CRC Press, 2009, pp.59–115.
12. National Research council. *Guide for the care and use of laboratory animals*. New York, NY: National Academies Press, 2010.
13. Bramhall M, Florez-Vargas O, Stevens R, et al. Quality of methods reporting in animal models of colitis. *Inflamm Bowel Dis* 2015; 21: 1248–1259.
14. Shih AY, Drew PJ, Mateo C, et al. A polished and reinforced thinned skull window for long-term imaging and optical manipulation of the mouse cortex. *J Visual Exp* 2012; 7: 3742.
15. Shih AY, Driscoll JD, Drew PJ, et al. Two-photon microscopy as a tool to study blood flow and neurovascular coupling in the rodent brain. *J Cereb Blood Flow Metab* 2012; 32: 1277–1309.
16. Driscoll JD, Shih AY, Drew PJ, et al. Two-photon imaging of blood flow in the rat cortex. *Cold Spring Harbor Protoc* 2013; 2013: 759–767.
17. Shih AY, Friedman B, Drew PJ, et al. Active dilation of penetrating arterioles restores red blood cell flux to penumbral neocortex after focal stroke. *J Cereb Blood Flow Metab* 2009; 29: 738–751.
18. Shih AY, Nishimura N, Nguyen J, et al. Optically induced occlusion of single blood vessels in rodent neocortex. *Cold Spring Harbor Protoc* 2013; 2013: 1153–1160.
19. Schindelin J, Arganda-Carreras I, Frise E, et al. Fiji: an open-source platform for biological-image analysis. *Nat Meth* 2012; 9: 676–682.
20. Schindelin J, Rueden CT, Hiner MC, et al. The ImageJ ecosystem: an open platform for biomedical image analysis. *Mol Reprod Develop* 2015; 82: 518–529.
21. Drew PJ, Blinder P, Cauwenberghs G, et al. Rapid determination of particle velocity from space-time images using the Radon transform. *J Comput Neurosci* 2010; 29: 5–11.
22. Capers PL, Hyacinth HI, Cue S, et al. Body composition and grip strength are improved in transgenic sickle mice fed a high-protein diet. *J Nutr Sci* 2015; 4: e6.
23. Hyacinth HI, Capers PL, Archer DR, et al. TNF-α, IFN-γ, IL-10, and IL-4 levels were elevated in a murine model of human sickle cell anemia maintained on

a high protein/calorie diet. *Exp Biol Med* 2014; 239: 65–70.
24. Manci EA, Hyacinth HI, Capers PL, et al. High protein diet attenuates histopathologic organ damage and vascular leakage in transgenic murine model of sickle cell anemia. *Exp Biol Med* 2014; 239: 966–974.
25. Arganda-Carreras I, Fernández-González R, Muñoz-Barrutia A, et al. 3D reconstruction of histological sections: application to mammary gland tissue. *Microsc Res Techn* 2010; 73: 1019–1029.
26. Doube M, Klosowski MM, Arganda-Carreras I, et al. BoneJ: free and extensible bone image analysis in ImageJ. *Bone* 2010; 47: 1076–1079.
27. Summers PM, Hartmann DA, Hui ES, et al. Functional deficits induced by cortical microinfarcts. *J Cereb Blood Flow Metab*. Epub ahead of print 1 January 2017. DOI: 10.1177/0271678X16685573.
28. Prohovnik I, Hurlet-Jensen A, Adams R, et al. Hemodynamic etiology of elevated flow velocity and stroke in sickle-cell disease. *J Cereb Blood Flow Metab* 2009; 29: 803–810.
29. Jordan LC, Casella JF and DeBaun MR. Prospects for primary stroke prevention in children with sickle cell anaemia. *Br J Haematol* 2012; 157: 14–25.
30. Angleys H, Jespersen SN and Ostergaard L. The effects of capillary transit time heterogeneity (CTH) on the cerebral uptake of glucose and glucose analogs: application to FDG and comparison to oxygen uptake. *Front Comput Neurosci* 2016; 10: 103.
31. Jespersen SN and Ostergaard L. The roles of cerebral blood flow, capillary transit time heterogeneity, and oxygen tension in brain oxygenation and metabolism. *J Cereb Blood Flow Metab* 2012; 32: 264–277.
32. Rasmussen PM, Jespersen SN and Ostergaard L. The effects of transit time heterogeneity on brain oxygenation during rest and functional activation. *J Cereb Blood Flow Metab* 2015; 35: 432–442.
33. Dobson SR, Holden KR, Nietert PJ, et al. Moyamoya syndrome in childhood sickle cell disease: a predictive factor for recurrent cerebrovascular events. *Blood* 2002; 99: 3144–3150.
34. Adams R, Aaslid R, el Gammal T, et al. Detection of cerebral vasculopathy in sickle cell disease using transcranial Doppler ultrasonography and magnetic resonance imaging. Case report. *Stroke* 1988; 19: 518–520.
35. Douce D, Soliman EZ, Naik RP, et al. Abstract P023: association of sickle cell trait with common electrocardiographic abnormalities in the reasons for geographic and racial differences in stroke (REGARDS) study. *Circulation* 2017; 135(Suppl 1): AP023.
36. Arvanitakis Z, Capuano AW, Leurgans SE, et al. The relationship of cerebral vessel pathology to brain microinfarcts. *Brain Pathol* 2017; 27(1): 77–85.
37. Hilal S, Chai YL, van Veluw S, et al. Association between subclinical cardiac biomarkers and clinically manifest cardiac diseases with cortical cerebral microinfarcts. *JAMA Neurol* 2017; 74: 403–410.
38. Smith EE, Schneider JA, Wardlaw JM, et al. Cerebral microinfarcts: the invisible lesions. *Lancet Neurol* 2012; 11: 272–282.
39. King AA, DeBaun MR and White DA. Need for cognitive rehabilitation for children with sickle cell disease and strokes. *Exp Rev Neurother* 2008; 8: 291–296.
40. King AA, Rodeghier MJ, Panepinto JA, et al. Silent cerebral infarction, income, and grade retention among students with sickle cell anemia. *Am J Hematol* 2014; 89: E188–E192.
41. King AA, Strouse JJ, Rodeghier MJ, et al. Parent education and biologic factors influence on cognition in sickle cell anemia. *Am J Hematol* 2014; 89: 162–167.
42. Taylor ZJ, Hui ES, Watson AN, et al. Microvascular basis for growth of small infarcts following occlusion of single penetrating arterioles in mouse cortex. *J Cereb Blood Flow Metab* 2016; 36: 1357–1373.